General Relativity with Double Pulsars

M. Kramer
Jodrell Bank Observatory, The University of Manchester, Jodrell Bank, Macclesfield SK11 9DL, UK

A new era in fundamental physics began with the discovery of pulsars 1967, the discovery of the first binary pulsar in 1974 and the first millisecond pulsar in 1982. Ever since, pulsars have been used as precise cosmic clocks, taking us beyond the weak-field regime of the solar-system in the study of theories of gravity. Their contribution is crucial as no test can be considered to be complete without probing the strong-field realm of gravitational physics by finding and timing pulsars. This is particularly highlighted by the discovery of the first double pulsar system. This first ever double pulsar, discovered by our team 18 months ago, consists of two pulsars, one with period of only 22 ms and the other with a period of 2.8 sec. This binary system with a period of only 2.4-hr provides a truly unique laboratory for relativistic gravitational physics.

1. Introduction

Rarely had the formulation of a single theory changed our view of the Universe so dramatically as Einstein's theory of general relativity (GR). Immediately after its publication, scientists were considering ways of testing GR to experimentally verify the revolutionary different effects that were predicted as deviations from Newton's theory of gravity which had ruled supreme for about three hundred years. Already during World War I., British scientists were planning two expeditions to test GR by observing a predicted bending of light around the Sun during a total solar eclipse to be observed in 1919 in Brazil and Africa. The expeditions indeed took place, and Sir Arthur Eddington himself analysed photographic plates taken during the eclipse that showed the apparent displacement of stars when they were positioned behind the Sun. This bending of light near massive bodies confirmed one of Einstein's predictions and propelled him to immediate global stardom. Today, 85 years after these historic observations, physicists are still trying to put GR to the test. One of the toughest tests ever has recently become possible by the discovery of two pulsars which are found to be in a close, slowly decaying orbit that will eventually lead to the destruction of these objects, predicted to happen in about 85 million years.

In this contribution I will review the basic properties of pulsars and how binary pulsars, and in particular the double pulsar, can be used to perform the most stringent tests of GR in the strong-field regime. The double pulsar system was found in a collaboration of two European groups, based at the Jodrell Bank Observatory of The University of Manchester in the UK and the Universities of Palermo and Bologna (more recently Cagliari Astronomical Observatory) in Italy, and Australian colleagues at the Australia Telescope National Facility, CSIRO, which is also operating the Parkes telescope that was instrumental in the discovery [1, 2]. I will conclude with a preview to the studies of relativistic gravity that will become possible with the future giant Square-Kilometre-Array telescope.

2. Pulsars

Pulsars are highly magnetised, rotating neutron stars which emit a narrow radio beam along the magnetic dipole axis. As the magnetic axis is inclined to the rotation axis, the pulsar acts like a cosmic light-house emitting a radio pulse that can be detected once per rotation period when the beam is directed toward Earth. For some very fast rotating pulsars, the so-called millisecond pulsars (see Sect. 4), the stability of the pulse period is similar to that achieved by the best terrestrial atomic clocks. Using these astrophysical clocks by accurately measuring the arrival times of their pulses, a wide range of experiments is possible, for which it is not necessarily important *how* the radio pulses are actually created. We will consider some of the basic pulsar properties below.

Pulsars are born in supernova explosions of massive stars. Created in the collapse of the stars' core, neutron stars are the most compact objects next to black holes. From timing measurements of binary pulsars (see Sect. 6), we determine the masses of pulsars to be typically around $1.35 \pm 0.04 M_\odot$ [3]. Modern calculations for different equations

of state produce results for the size of a neutron star quite similar to the very first calculations by Oppenheimer & Volkov [4], i.e. about 20 km in diameter. Such sizes are consistent with independent estimates derived from X-ray light-curves and luminosities of pulsars (e.g. [5]).

Pulsars emit electromagnetic radiation and, in particular, magnetic dipole radiation as they essentially represent rotating magnets. Assuming that this is the dominant effect for an increase in rotation period, P, described by $\dot{P}$, we can equate the corresponding energy output of the dipole to the loss rate in rotational energy. We obtain an estimate for the magnetic field strength at the pulsar (equatorial) surface from

$$B_S = 3.2 \times 10^{19} \sqrt{P\dot{P}} \text{ Gauss}, \tag{1}$$

with P measured in s and $\dot{P}$ in s s^{-1}. Millisecond pulsars have lower field strengths of the order of 10^8 to 10^{10} Gauss which appear to be a result of their evolutionary history (see Section 4). These magnetic fields are consistent with values derived from X-ray spectra of neutron stars where we observe cyclotron lines [6].

The radio signal of a pulsar is usually weak, both because the pulsar is distant and the size of the actual emission region is small. Estimates range down to a few metres, resulting in brightness temperatures of up to 10^{37} K [7]. Such values require a coherent emission mechanism which, despite 37 years of intensive research, is still unidentified. However, we seem to have some basic understanding, in which the magnetised rotating neutron star induces an electric quadrupole field which is strong enough to pull out charges from the stellar surface (the electrical force exceeds the gravitational force by a factor of $\sim 10^{12}$!). The magnetic field forces the resulting dense plasma to co-rotate with the pulsar. This *magnetosphere* can only extend up to a (maximum) distance where the co-rotation velocity reaches the speed of light. This distance defines the so-called light cylinder which separates the magnetic field lines into two distinct groups, i.e. *open and closed field lines*. The plasma on the closed field lines is trapped and co-rotates with the pulsar forever. In contrast, plasma on the open field lines can reach highly relativistic velocities and can leave the magnetosphere; the observed radio beam is created in the polar region at a distance of a few tens to hundreds of km above the pulsar surface.

Most pulsars are not strong enough for us to allow studies of their individual radio pulses. Then, only an integrated pulse shape, the "pulse profile", can be observed. Individual pulses reflect the instantaneous plasma processes in the pulsar magnetosphere, resulting in often seemingly random pulses. In contrast, the average pulse profile reflects the global constraints mostly given by a conal beam structure and geometrical factors and is thereby stable. It is this profile stability which allows us to time pulsar to high precision.

3. Evolution of Pulsars

The evolution in pulsar period, P, and slow-down, $\dot{P}$, can be used to describe the life of a pulsar. This is usually done in a (logarithmic) P-$\dot{P}$-diagram as shown in Figure 1 where we can draw lines of constant magnetic field (see Eqn. 1) and constant "characteristic age" estimated from

$$\tau = \frac{P}{2\dot{P}}. \tag{2}$$

This quantity is a valid estimate for the true age if spin-down is indeed fully determined by magnetic dipole braking and if the initial spin period, P_0, is much smaller than the present period, P. Until recently, it was believed that pulsars are born with periods similar to that estimated for the Crab pulsar at birth, $P_0 = 19$ ms [8]. However, new estimates for a growing number of pulsars suggest a wide range of initial spin periods from 14 ms up to 140 ms [9]. Pulsars are therefore born in a wider region located the upper left area of Fig. 1 from which they move into the central part where they spent most of their lifetime.

In the central part of the $P - \dot{P}$-diagram, pulsars have spin periods between 0.1 and 1.0 s and period derivatives of typically $\dot{P} = 10^{-15}$ s s^{-1}. Selection effects are only partly responsible for the limited number of pulsars known with very long periods, the longest known period being 8.5 s [10]. The dominant effect is the "death" of pulsars when their slow-down has reached a critical state. This state seems to depend on a combination of P and $\dot{P}$ which can

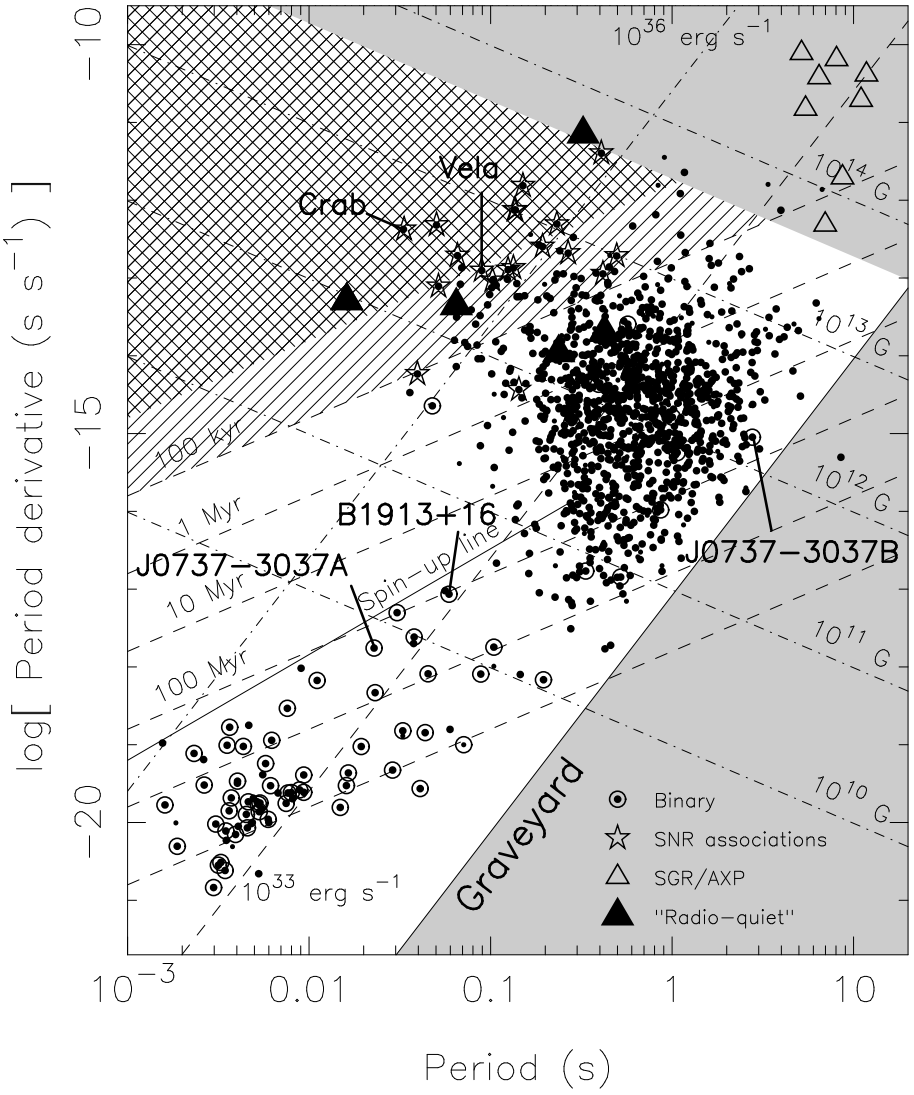

Figure 1: The $P-\dot{P}$–diagram for the known pulsar population. Lines of constant characteristic age, surface magnetic field and spin-down luminosity are shown. Binary pulsars are marked by a circle. The lower solid line represents the pulsar "death line" enclosing the "pulsar graveyard" where pulsars are expected to switch off radio emission. The grey area in the top right corner indicates the region where the surface magnetic field appears to exceed the quantum critical field of 4.4×10^{13} Gauss. For such values, some theories expect the quenching of radio emission in order to explain the radio-quiet "magnetars" (i.e. Soft-gamma ray repeaters, SGRs, and Anomalous X-ray pulsars, AXPs). The upper solid line is the "spin-up" line which is derived for the recycling process as the period limit for millisecond pulsars.

be represented in the $P-\dot{P}$-diagram as a "pulsar death-line". To the right and below this line (see Figure 1) the electric potential above the polar cap may not be sufficient to produce the particle plasma that is responsible for the observed radio emission. While this model can indeed explain the lack of pulsars beyond the death-line, the truth may be more complicated as the position of the 8.5-sec pulsar deep in the "pulsar graveyard" indicates. Nevertheless, it is clear that the normal life of radio pulsars is limited and that they die eventually after tens to a hundred million years.

4. Formation of Millisecond Pulsars

The evolution of pulsars described above does not explain the origin of a sub-set of about 100 pulsars located in the lower left part of the $P - \dot{P}$-diagram. These pulsars, called millisecond pulsars because of their small periods, also have very small period derivatives, $\dot{P} \lesssim 10^{-18}$ s s^{-1}, making them much older (see Eqn. 2) than normal pulsars with ages up to $\sim 10^{10}$ yr. In the standard scenario, which finds its ultimate confirmation in the discovery of the double pulsar, millisecond pulsars are recycled from a dead binary pulsar via an X-ray binary accretion phase. The pulsars' millisecond periods are obtained when mass and thereby angular momentum is transferred from an evolving binary companion while it overflows its Roche lobe (e.g. [11]).

Even though most ordinary stars are in binary systems, most pulsars do not evolve into a millisecond pulsar. The birth of the pulsar usually disrupts the system, preventing the access to a mass donor and explaining why most pulsars are isolated. In the binary systems that survive the supernova explosion, the pulsar will eventually cease to emit radio emission, before the system evolves into a X-ray binary phase during which mass accretion onto the pulsar occurs. The pulsar spins up and is recycled into a radio millisecond pulsar when P and $\dot{P}$ have been altered such that the pulsar has crossed the death-line again in the other direction. The final spin period of such a recycled pulsar depends on the mass of the binary companion. A more massive companion evolves faster, limiting the duration of the accretion process and hence the angular momentum transfer.

The majority of millisecond pulsars will have had a low-massive companion. These systems evolve into low-mass X-ray binaries (LMXBs) and will result into a fast-spinning millisecond pulsar with period of $P \sim 1 - 10$ms with a low-mass white-dwarf companion. Systems with a more massive companion evolve into high-mass X-ray binaries (HMXBs) which represent the progenitors for double neutron star systems (DNSs). DNSs are rare since these systems need to survive a total of two supernova explosions. If this happens, the millisecond pulsar is only mildly recycled with a period of tens of millisecond.

The properties of millisecond pulsars and X-ray binaries are consistent with the described picture. For instance, it is striking that $\sim 80\%$ of all millisecond pulsars are in a binary orbit while this is true for only less than 1% of the non-recycled population. For millisecond pulsars with a low-mass white dwarf companion the orbit is nearly circular due to a circularisation of the orbit during the recycling process. In case of DNS systems, the orbit is affected by the unpredictable nature of the kick imparted onto the newly born neutron star in the asymmetric supernova explosion of the companion. If the system survives, the result is typically an eccentric orbit with an orbital period of a few hours.

5. Pulsar Timing

The clock-like stability of pulsars means that through precise monitoring of pulsar rotations we can study a rich variety of phenomena that affect the propagation of their pulses. While the basic spin and astrometric parameters can be derived for essentially all pulsars, millisecond pulsars are the most useful objects for more exotic applications. Their pulse arrival times can be measured much more precisely than for normal pulsars (scaling essentially with the pulse period) and their rotation is also much smoother, making them intrinsically better clocks. Specifically, they usually do not exhibit rotational instabilities such as 'timing noise' and 'glitches' known for normal pulsars.

The key quantity of interest is the *time of arrival* (TOA) of pulses at the telescope. However, since individual pulses are usually too weak to be detected, and since they also show a jitter in arrival time within a window given by the extend of the pulse profile, it is the latter which is used for timing. The stability of pulse profiles allows us to compare the observed profile with a high signal-to-noise ratio template that is constructed from previous observations. The time-offset between template and profile determines the TOA. Because we use pulse profiles rather than individual pulses, the TOA is defined usually as the arrival time of the nearest pulse to the mid-point of the observation. As the pulses have a certain width, the TOA refers to some *fiducial point* on the profile. Ideally, this point coincides with the plane defined by the rotation and magnetic axes of the pulsar and the line of sight to the observer which is defined geometrically and independent of observing frequency or propagation effects.

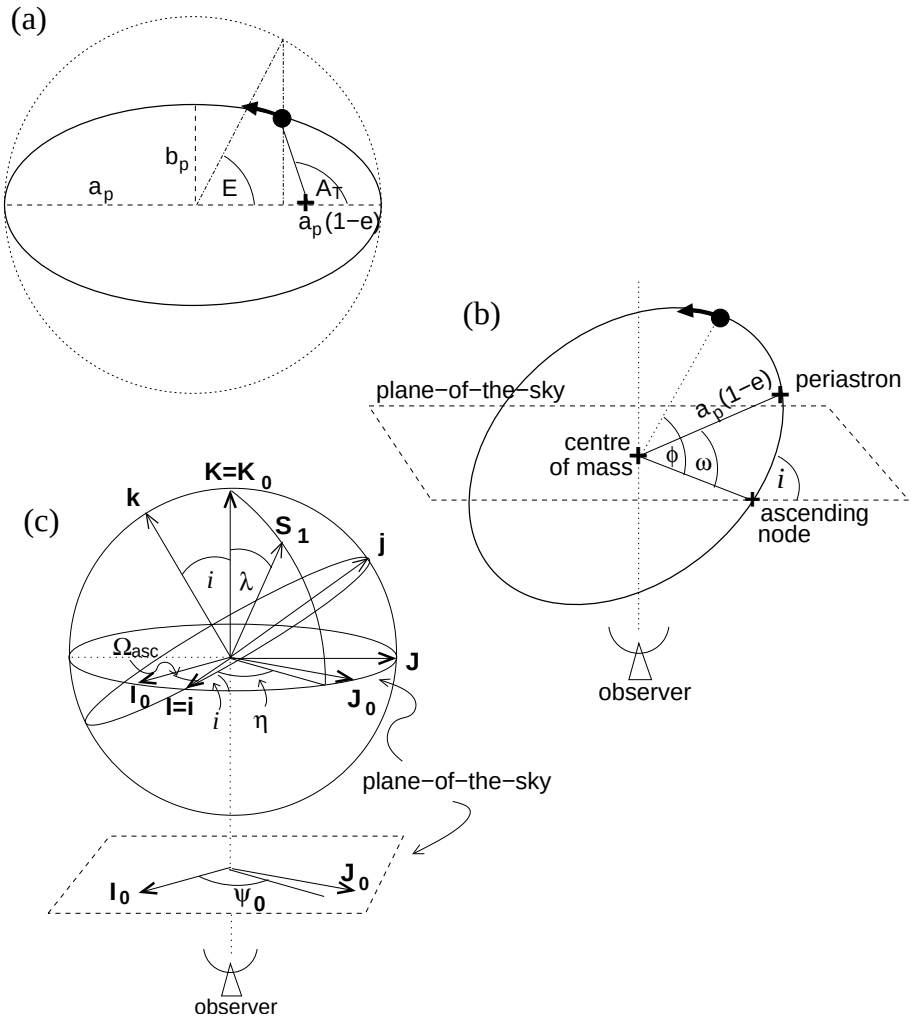

Figure 2: Definition of the orbital elements in a Keplerian orbit and the angles relating both the orbit and the pulsar to the observer's coordinate system and line of sight. (a) is drawn in the plane of the orbit; (b) shows the orbit inclined to the plane of the sky. The closest approach of the pulsar to the centre of mass of the binary system marks periastron, given by the longitude ω and a chosen epoch T_0 of its passage. The distance between centre of mass and periastron is given by $a_{\rm p}(1-e)$ where $a_{\rm p}$ is the semi-major axis of the orbital ellipse and e its eccentricity. (b) Usually, only the projection on the plane of the sky, $a_{\rm p}\sin i$, is measurable, where i is the orbital inclination defined as the angle between the orbital plane and the plane of the sky. The *true anomaly*, $A_{\rm T}$, and *eccentric anomaly*, E, are related to the *mean anomaly* by Kepler's law. The orbital phase of the pulsar Φ is measured relative to the ascending node. (c) The spatial orientation of the pulsar's spin-vector, $\mathbf{S_1}$, is given by the angles λ and η in the coordinate system shown as defined by Damour and Taylor (1992). The angle $\Omega_{\rm asc}$ gives the longitude of ascending node in the plane of the sky.

The aim of pulsar timing is to count the number of neutron star rotations between two observations. Each TOA can therefore be assigned with a pulse number N which depends on rotation frequency ν and TOA t as

$$N = N_0 + \nu_0(t-t_0) + \frac{1}{2}\dot{\nu}(t-t_0)^2 + \frac{1}{6}\ddot{\nu}(t-t_0)^3 + \cdots \tag{3}$$

where N_0 is the pulse number at the reference epoch t_0. If t_0 coincides with the arrival of a pulse and the pulsar spin-down (i.e. ν and $\dot{\nu}$) is known accurately, the pulses should appear at integer values of N when observed in an inertial reference frame. However, our observing frame is not inertial: we are using telescopes that are located on a rotating Earth orbiting the Sun. Before analysing TOAs measured with the observatory clock ('topocentric arrival times'), we need to transfer them to the centre of mass of the Solar System (solar system barycentre, SSB). To a

very good approximation, the SSB is an inertial reference frame.

The time transformation also corrects for any relativistic time delay that occurs due to the presence of masses in the Solar System. An additional advantage of analysing these 'barycentric arrival times' is that they can easily be combined with other TOAs measured at different observatories at different times.

6. Binary Pulsars

Observations of pulsars in binary orbits show a periodic variation in pulse arrival time. The timing model therefore needs to incorporate the additional motion of the pulsar as it orbits the common centre of mass of the binary system. For non-relativistic binary systems, the orbit can be described using Kepler's laws. For a number of binary systems however, the Keplerian description of the orbit is not sufficient and relativistic corrections need to be applied.

Kepler's laws can be used to describe a binary system in terms of so-called 'Keplerian parameters', shown schematically in Figure 2. Five parameters are required to refer the TOAs to the binary barycentre: (a) orbital period, $P_{\rm b}$; (b) projected semi-major orbital axis, $a_{\rm p} \sin i$ (see below); (c) orbital eccentricity, e; (d) longitude of periastron, ω; (e) the epoch of periastron passage, T_0.

For pulsars in close binary systems about white dwarfs, other neutron stars, or perhaps eventually black holes, relativistic effects due to strong gravitational fields and high orbital velocities produce observable signatures in the timing residuals. Even though GR appears to be the best description of the strong-field regime to date [12], alternative theories of gravity nevertheless should be considered and tested against it. A straightforward means of comparison is to parameterise the timing model in terms of the so-called 'post-Keplerian' (PK) parameters. For point masses with negligible spin contributions, the PK parameters in each theory should only be functions of the a priori unknown pulsar and companion mass, $M_{\rm p}$ and $M_{\rm c}$, and the easily measurable Keplerian parameters [13]. With the two masses as the only free parameters, an observation of two PK parameters will already determine the masses uniquely in the framework of the given theory. The measurement of a third or more PK parameters then provides a consistency check for the assumed theory.

In general relativity, the five most important PK parameters are given by (e.g. [13]):

$$\dot{\omega} = 3T_{\odot}^{2/3} \left(\frac{P_{\rm b}}{2\pi}\right)^{-5/3} \frac{1}{1-e^2} (M_{\rm p}+M_{\rm c})^{2/3}, \tag{4}$$

$$\gamma = T_{\odot}^{2/3} \left(\frac{P_{\rm b}}{2\pi}\right)^{1/3} e \frac{M_{\rm c}(M_{\rm p}+2M_{\rm c})}{(M_{\rm p}+M_{\rm c})^{4/3}}, \tag{5}$$

$$\dot{P}_{\rm b} = -\frac{192\pi}{5} T_{\odot}^{5/3} \left(\frac{P_{\rm b}}{2\pi}\right)^{-5/3} \frac{\left(1+\frac{73}{24}e^2+\frac{37}{96}e^4\right)}{(1-e^2)^{7/2}} \frac{M_{\rm p}M_{\rm c}}{(M_{\rm p}+M_{\rm c})^{1/3}}, \tag{6}$$

$$r = T_{\odot} M_{\rm c}, \tag{7}$$

$$s = T_{\odot}^{-1/3} \left(\frac{P_{\rm b}}{2\pi}\right)^{-2/3} x \frac{(M_{\rm p}+M_{\rm c})^{2/3}}{M_{\rm c}}, \tag{8}$$

where the masses M_p and M_c of pulsar and companion, respectively, are expressed in solar masses ($M_\odot$). We define the constant $T_\odot = GM_\odot/c^3 = 4.925490947\mu$s where G denotes the Newtonian constant of gravity and c the speed of light. The first PK parameter, $\dot{\omega}$, is the easiest to measure and describes the relativistic advance of periastron. It provides an immediate measurement of the total mass of the system, $(M_{\rm p}+M_{\rm c})$. The parameter γ denotes the amplitude of delays in arrival times caused by the varying effects of the gravitational redshift and time dilation (second order Doppler) as the pulsar moves in its elliptical orbit at varying distances from the companion and with varying speeds. The decay of the orbit due to gravitational wave damping is expressed by the change in orbital period, $\dot{P}_{\rm b}$. The other two parameters, r and s, are related to the Shapiro delay caused by the gravitational field of the companion. These parameters are only measurable, depending on timing precision, if the orbit is seen nearly edge-on.

7. The Double Pulsar System: PSR J0737−3039A & PSR J0737−3039B

Our team discovered the 22.8-ms pulsar J0737-3039 in April 2003 [1] in an extension to the hugely successful Parkes Multi-beam survey [14]. It was soon found to be a member of the most extreme relativistic binary system ever discovered: its short orbital period ($P_{\rm b}$ = 2.4 hrs) is combined with a remarkable high value of periastron advance ($\dot{\omega}$ = 16.9 deg/yr, i.e. four times larger than for PSR B1913+16!) that was measurable after only a few days of observations. The system parameters predict that the two members of the binary system will coalesce on a remarkably short time scale of only $\sim$ 85 Myr. This boosts the hopes for detecting a merger of two neutron stars with first-generation ground-based gravitational wave detectors by about an order of magnitude compared to previous estimates based on only the DNSs B1534+12 and B1913+16 [1, 15].

In October 2003, we detected radio pulses from the second neutron star when data sets covering the full orbital period were analysed [2]. The reason why signals from the 2.8-s pulsar companion (now called PSR J0737−3039B, hereafter "B") to the millisecond pulsar (now called PSR J0737−3039A, hereafter "A") had not been found earlier, became clear when it was realized that B was only visible clearly for two short parts of the orbits. For the remainder of the orbit, the pulsar B is extremely weak and only detectable with the most sensitive equipment. The detection of a young pulsar-companion B clearly confirmed the evolution scenario presented in Section 4 and made this already exciting system sensational, providing a truly unique testbed for relativistic gravity.

Indeed, in addition to the already measured $\dot{\omega}$ and γ for A, we have also detected the Shapiro delay in the pulse arrival times of A due to the gravitational field of B, providing a precise measurement of the orbital inclination of $\sin i = 0.9995(^{-32}_{+4})$. Obviously, as another strike of luck, we are observing the system almost completely edge-on which allows us to also probe pulsar magnetospheres for the very first time by a background beacon. In the following, I will present some of the latest results on both the interaction between A and B, as well as on tests of general relativity.

Table I: Observed and derived parameters of PSRs J0737−3039A and B. Standard errors are given in parentheses after the values and are in units of the least significant digit(s).

Pulsar	PSR J0737−3039A	PSR J0737−3039B
Pulse period P (ms)	22.69937855615(6)	2773.4607474(4)
Period derivative $\dot{P}$	$1.74(5) \times 10^{-18}$	$0.88(13) \times 10^{-15}$
Epoch of period (MJD)	52870.0	52870.0
Right ascension α (J2000)	$07^{\rm h}37^{\rm m}51^{\rm s}.2473(6)$	
Declination δ (J2000)	$-30°39'40''.729(9)$	
Orbital period $P_{\rm b}$ (day)	0.1022515629(4)	
Eccentricity e	0.087778(1)	
Epoch of periastron T_0 (MJD)	52870.0120588(4)	
Advance of periastron $\dot{\omega}$ (deg/yr)	16.900(5)	
Longitude of periastron ω (deg)	73.804(2)	73.805 + 180.0
Projected semi-major axis $x = a\sin i/c$ (sec)	1.415037(5)	1.513(4)
Gravitational redshift parameter γ (ms)	0.36(2)	
Shapiro delay parameter $s = \sin i$	$0.9995(-32, +4)$	
Shapiro delay parameter r (μs)	$5.6(-12, +18)$	
Orbital decay $\dot{P}_{\rm b}$ (10^{-12})	−1.2(4)	
Mass ratio $R = m_{\rm A}/m_{\rm B}$	1.068(2)	
Orbital inclination from Shapiro s (deg)	88(1)	
Total system mass $m_{\rm A} + m_{\rm B}$ ($M_\odot$)	2.587(4)	
Stellar mass ($M_\odot$)	1.336(2)	1.251(2)
Geodetic precession rate (deg/yr)	4.79	5.07

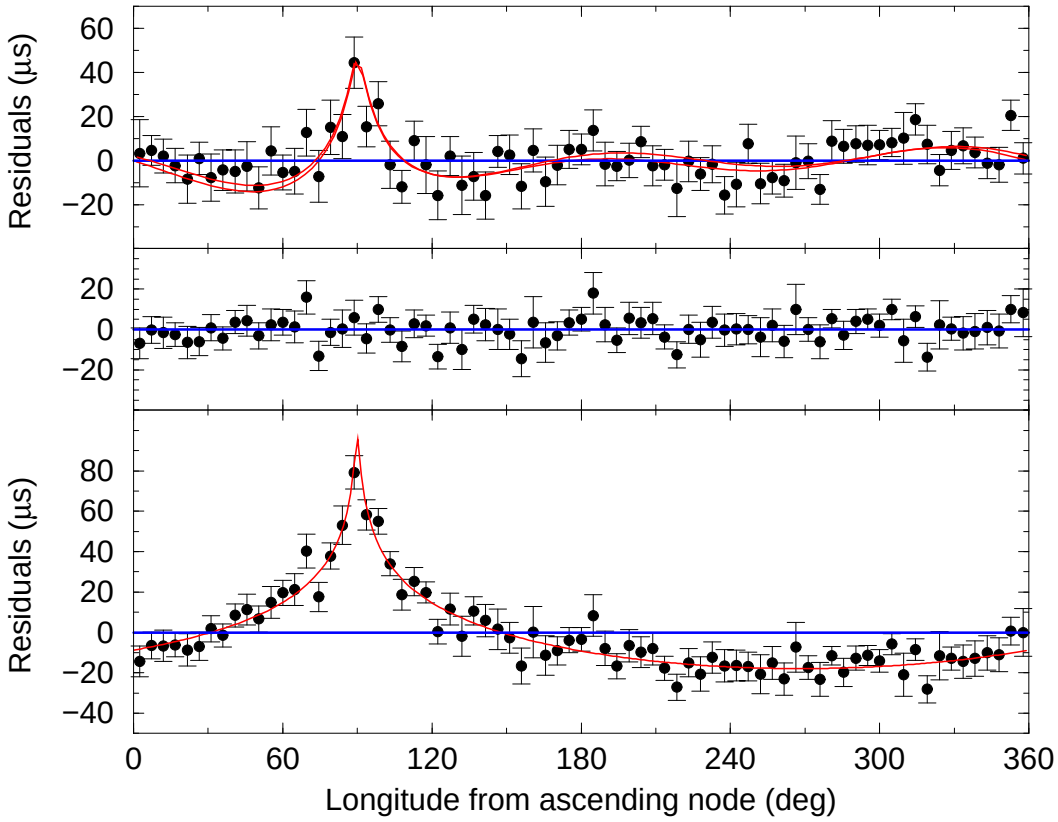

Figure 3: The effect of the Shapiro delay caused by the gravitational potential of B seen in the timing residuals of A. Top: timing residuals obtained by fitting all model parameters shown in Table 1 except the Shapiro delay parameters r and s. The left-over structure represents the higher harmonics of the Shapiro delay that are unabsorbed by fits to the Keplerian parameters. Middle: Timing residuals after fitting additionally for the Shapiro delay. Bottom: as middle display, but with the Shapiro delay parameters r and s set to zero.

7.1. Tests of General Relativity

Our observations already provide measurements for all five PK parameters listed above. As indicated earlier, we can use these results to test GR in a very elegant way [13]. For each PK parameter, GR (or any other theory) predicts a unique relationship between the two masses of the system. By plotting each of these relationships in a diagram showing the mass of A on one axis and B on the other, we expect all curves to intersect in a single point if the chosen theory (here GR) is a valid description of the nature of this system. Such tests have been possible to date in only two double neutron star systems, PSR B1913+16 (e.g. [16]) and for PSR B1534+12 (e.g. [17]). However, in none of these systems were so many curves available as for the double pulsar system for which we derive a $m_A - m_B$ plot as shown in Fig. 4.

While the orbital decay due to gravitational wave emission is already detected clearly, the measurement uncertainties are yet too large to provide a useful constraint. In particular, one should note that the observed value of $\dot{P}_{\rm b}$ is positively biased by a contribution arising from a relative motion and acceleration. Very long baseline interferometry observations are underway to measure both proper motion and distance of the system independently of pulsar timing. This will allow us to interpret the observed $\dot{P}_{\rm b}$ value in the context of gravitational theories.

While the error bars on all PK parameters are decreasing with time, the detection of B as a pulsar opens up opportunities that go well beyond what has been possible in GR tests so far. With a measurement of the projected semi-major axes of the orbits of both A and B, we obtain a precise measurement of the mass ratio, $R(m_{\rm A}, m_{\rm B}) \equiv m_{\rm A}/m_{\rm B} = x_{\rm B}/x_{\rm A}$, providing a further constraint displayed in Fig. 4. For every realistic theory of gravity, we

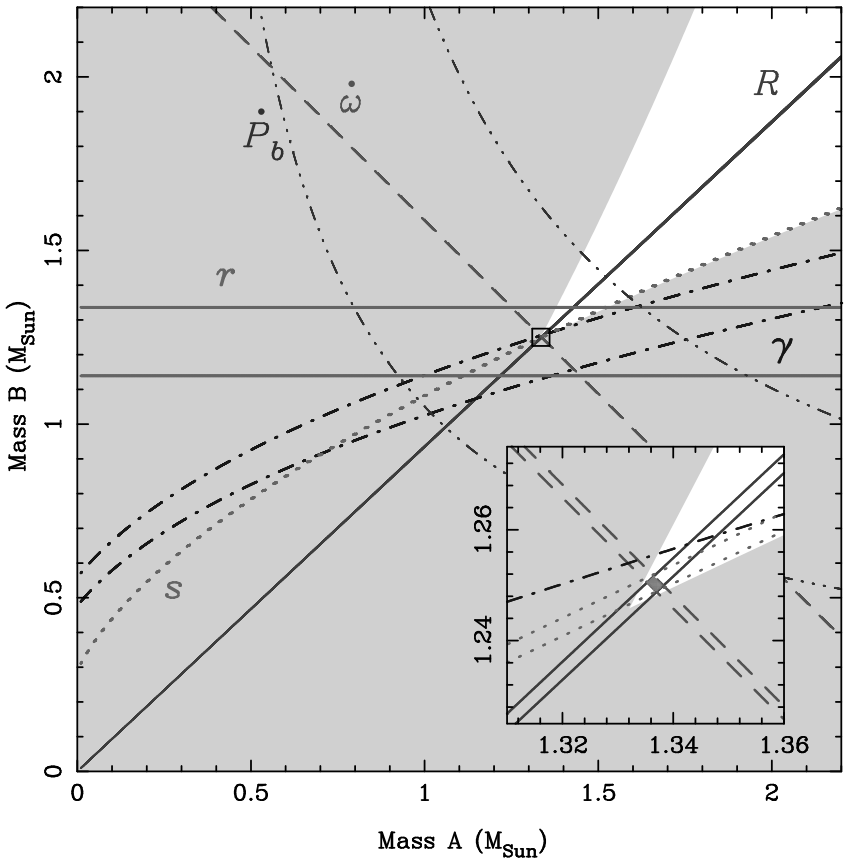

Figure 4: 'Mass–mass' diagram showing the observational constraints on the masses of the neutron stars in the double pulsar system J0737–3039. The shaded regions are those that are excluded by the Keplerian mass functions of the two pulsars. Further constraints are shown as pairs of lines enclosing permitted regions as predicted by general relativity: (a) the measurement of $\dot{\omega}$ gives the total system mass $m_{\rm A} + m_{\rm B} = 2.59$ M$_\odot$; (b) the measurement of the mass ratio $R = m_{\rm A}/m_{\rm B} = 1.07$; (c) the measurement of the gravitational redshift/time dilation parameter γ; (d) the measurement of the two Shapiro delay parameters r and s; (e) the detection of an orbital decay, $\dot{P}_{\rm b}$, due to gravitational wave emission, indicating that the orbit is shrinking by about 7mm every day. Inset is an enlarged view of the small square encompassing the intersection of the three tightest constraints (see text).

can expect the mass ratio, R, to follow this simple relation [13]. Most importantly, the R-line is not only theory-independent, but also independent of strong-field (self-field) effects which is not the case for PK-parameters. This provides a stringent and new constraint for tests of gravitational theories as any intersection of the PK-parameters *must* be located on the R-line. At the same time, it provides us already with very accurate mass measurements for the neutron stars, $M_A = (1.336 \pm 0.002) M_\odot$ and $M_B = (1.251 \pm 0.002) M_\odot$, respectively, making B the least-massive neutron star ever observed. The current data indicate an agreement of the observed with the expected Shapiro parameter of $s_{\rm obs}/s_{\rm exp} = 1.000 \pm 0.002$ (Kramer et al. in prep.) where the uncertainties are certain to decrease.

7.2. A Magnificent Laboratory for Plasma Physics

The double pulsar is not only a superb test-bed for relativistic gravity, but it also provides an unprecedented opportunity to probe the workings of pulsars. The pulse emission from B is strongly modulated with orbital phase, most probably as a consequence of the penetration of the A's wind into B's magnetosphere. Figure 5 shows the pulse intensity for B as a function of pulse phase and orbital longitude for three radio frequencies. The first burst of strong

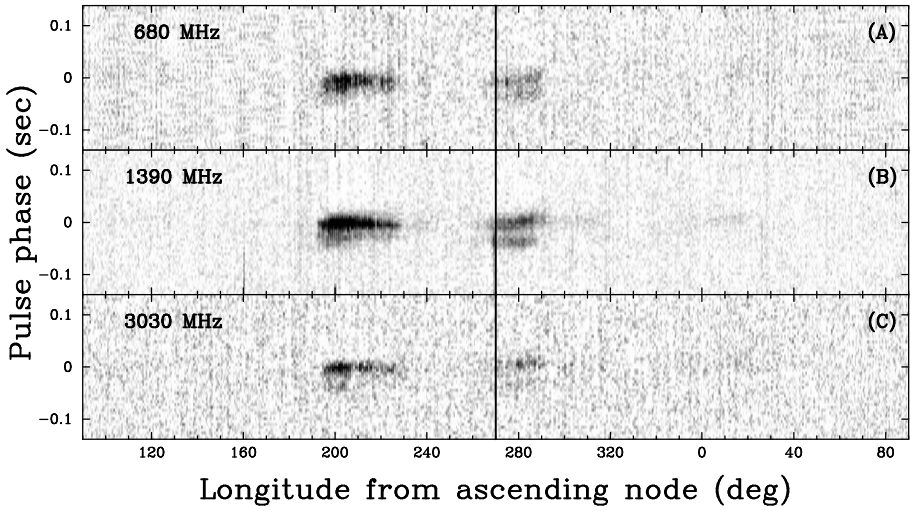

Figure 5: Grey-scale images showing the pulse of PSR J0737–3039B as a function of orbital phase at three observing frequencies (Lyne *et al.* 2004).

emission, centred near orbital longitude 210 deg, covers about 13 min of the orbit, while the second burst, centred near longitude 280 deg, is shorter and last only for about 8 min. This pattern is stable over successive orbits and obviously frequency independent over the range probed. Deep integrations reveal other orbital phases, where B is visible but much weaker than during the two main burst periods. The figure also shows that not only does the pulse intensity change with orbital phase, but that the pulse shape changes as well. At the start of the first burst the pulse has a strong trailing component and a weaker leading component which dies out in the later phases of the burst. In the second burst, there are two components of more equal amplitude. This is the first time that profile changes are observed that clearly depend on orbital phase. Decoding this pattern as the orbit precesses due to relativistic effects and the system is viewed from different directions, offers a unique chance to probe the magnetosphere, for instance by locating the region where the radio emission is created. The fact that B is still emitting despite the loss of most of its outer magnetosphere due to A's wind, already indicates that the fundamental processes producing radio emission are likely to occur close to the neutron star surface – in accordance with emission heights determined for normal radio pulsars (e.g. [18]).

The quenching or attenuation of B's radio emission for most of its orbit is only part of the interaction between A and B that is observed. For about 30 s of the orbit, A's emission is eclipsed when A is lined up behind B at superior conjunction. At that moment, the pulses of A pass in less than 50,000km distance to the surface of B. It is likely that A's emission is blocked by some of B's plasma in its magnetosphere, and indeed, modulation inside the eclipse region consistent with B's rotation period is observed [19]. Detailed studies will therefore allow us to probe plasma densities in pulsar magnetospheres for the first time.

Perhaps even more exciting is the discovered evidence that A's radiation has some direct impact on the radiation pattern of B. Figure 6 shows a blow-up of B's emission at orbital phases where B is strongest. At the right orientation angles, a drifting sub-pulse pattern emerges that coincides with the arrival times of A's pulses at B [20]. This is the first time pulsar emission is observed to be triggered by some external force, and it is likely that this will help us to understand the conditions and on-set of pulsar emission in general.

7.3. Future Tests of GR with the Double Pulsar

In GR, the proper reference frame of a freely falling object suffers a precession with respect to a distant observer, called geodetic precession. In a binary pulsar system this geodetic precession leads to a relativistic spin-orbit coupling, analogous of spin-orbit coupling in atomic physics [21]. As a consequence, the pulsar spin precesses about the

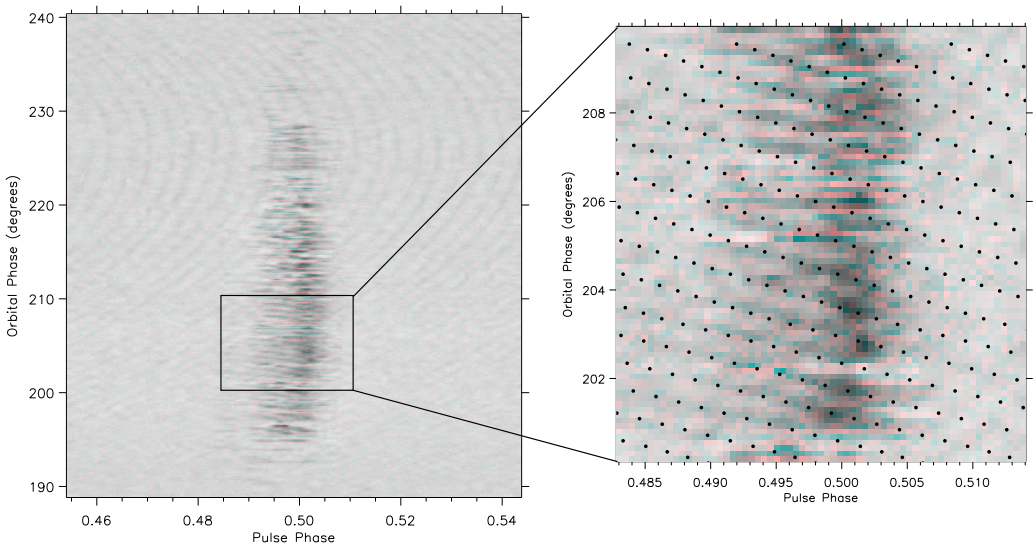

Figure 6: Observations of single pulses of B at 820 MHz for orbital phases 190 – 240 deg (only 10% of the pulse period is shown). Drifting features are present through most of these data, but are particularly obvious from orbital phases $\sim$ 200 – 210deg which is enlarged on the right. Single pulses of A can be seen in the background of the left figure, where differential Doppler shifts from the orbital motion result in different apparent pulse periods and hence drifting patterns. The expanded view on the right is overlayed with dots marking the arrival of pulses of A at the centre of B, coinciding with the observed drift pattern in B. (McLaughlin et al. 2004b)

total angular momentum, changing the relative orientation of the pulsar toward Earth. Since the orbital angular momentum is much larger than the pulsar spins, the total angular momentum is practically represented by the orbital spin. The precession rate [22] depends on the period and the eccentricity of the orbit as well as the pulsar and companion mass. With the parameters shown in Table 1, general relativity predicts precession periods of only 75 yr for A and 71 yr for B.

Geodetic precession should have a direct effect on the timing as it causes the polar angles of the spins and hence the effects of aberration to change with time [13]. These changes modify the *observed* orbital parameters, like projected semi-major axis and eccentricity, which differ from the *intrinsic* values by an aberration dependent term, potentially allowing to infer the system geometry. Other consequences of geodetic precession can be expected to be detected much sooner. These arise from changes in the pulse shape and its polarisation properties due to changing cuts through the emission beam as the pulsar spin axis precesses. Due to these effects, which may complicate the TOA determination, geodetic precession is detected for PSRs B1913+16 [23]. For PSR B1913+16 it is used to derive a two-dimensional map of the emission beam [24] and to determine the full system geometry leading to the prediction that the pulsar will not be observable from Earth around 2025 [23]. Since the precession rates for A and B are about four times larger, the visible effects in J0737−3039 should be much easier to detect.

The equations for the PK parameters given in Section 6 are all given to lowest Post-Newtonian order. However, higher-order corrections may become important if relativistic effects are large and timing precision is sufficiently high. Whilst this has not been the case in the past, the double pulsar system may allow measurements of these effects in the future [2]. One such effect involves the prediction by general relativity that, in contrast to Newtonian physics, the neutron stars' spins affect their orbital motion via spin-orbit coupling. This effect would be visible clearest as a contribution to the observed $\dot{\omega}$ in a secular [22] and periodic fashion [25]. For the J0737−3039 system, the expected contribution is about an order of magnitude larger than for PSR B1913+16, i.e. 2×10^{-4} deg yr^{-1} (for A, assuming a geometry as determined for PSR B1913+16 [23]). As the exact value depends on the pulsars' moment of inertia, a potential measurement of this effect allows the moment of inertia of a neutron star to be determined for the first time [26].

If two parameters, e.g. the Shapiro parameter s and the mass ratio R can be measured sufficiently accurate, an expected $\dot{\omega}_{\rm exp}$ can be computed from the intersection point. This value can be compared to the observed value $\dot{\omega}_{\rm obs}$ which is given by (see [26])

$$\dot{\omega}_{\rm obs} = \dot{\omega}_{\rm 1PN} \ \left[1 + \Delta\dot{\omega}_{\rm 2PN} - g^A \Delta\dot{\omega}^A_{\rm SO} - g^B \Delta\dot{\omega}^B_{\rm SO}\right] \tag{9}$$

where the last two terms represent contributions from the pulsar spin. In these terms, $g^{A,B}$ are geometry dependent factors whilst $\Delta\dot{\omega}^{A,B}_{\rm SO}$ arise from relativistic spin-orbit coupling, formally at the same level of first post-Newtonian approximation. However, it turns out that for binary pulsars these effects have a magnitude equivalent to second post-Newtonian order [25], so that they only need to be considered if $\dot{\omega}$ is to be studied at this higher level of approximation. We find $\Delta\dot{\omega}_{\rm SO} \propto I/Pm^2$ [26], so that with precisely measured masses m the moment of inertia I can be measured and the neutron star "equation-of-state" and our understanding of matter at extreme pressure and densities can be tested.

The dependence of $\Delta\dot{\omega}_{\rm SO}$ on the spin period P suggests that only a measurement for pulsar A can be obtained. It also requires that the at least two other parameters can be measured to a similar accuracy as $\dot{\omega}$. Despite being a tough challenge, e.g. due to the expected profile variation caused by geodetic precession, the prospect are promising. Simulations indicate that a few years of high precision timing are sufficient.

8. Tests with the Square-Kilometre-Array (SKA) using Pulsars and Black Holes

The Square-Kilometre-Array (SKA) will be a radio telescope with a collecting area that will exceed that of existing telescopes by a factor of a hundred or so. Through its sensitivity, sky and frequency coverage, the SKA will discover a very large fraction of the pulsars in the Galaxy, resulting in about 20,000 pulsars. This number represents essentially all active pulsars that are beamed toward Earth and includes the discovery of more than 1,000 millisecond pulsars (MSPs). This impressive yield effectively samples every possible outcome of the evolution of massive binary stars. The sensitivity of the SKA allows much shorter integration times, so that searches for compact binary pulsars will no longer be limited by Doppler-smearing of the observed pulse period. Among the discovered sources, pulsar-black hole (PSR-BH) systems are to be expected. Being timed with the SKA, a PSR-BH system would be an amazing probe of relativistic gravity with a discriminating power that surpasses all of its present and foreseeable competitors [27].

As stars rotate, astrophysicists also expect BHs to rotate, giving rise to both a BH spin and quadrupole moment. The resulting gravito-magnetic field causes a relativistic frame-dragging in the BH vicinity, leading the orbit of any test mass about the BH to precess if the orbit deviates from the equatorial plane. The consequences for timing a pulsar around a BH have been studied in detail [28], showing that the study of the orbital dynamics allows us to use the orbiting pulsar to probe the properties of the rotating BH. Not only can the mass of the BH be measured with very high accuracy, but the spin of the BH can also be determined precisely using the nonlinear-in-time, secular changes in the observable quantities due to *relativistic* spin-orbit coupling. The anisotropic nature of the quadrupole moment of the external gravitational field will produce characteristic short-term periodicities due to *classical* spin-orbit coupling, every time the pulsar gets close to the oblate BH companion [28, 29]. Therefore, the mass, M, and both the dimensionless spin χ and quadrupole q,

$$\chi \equiv \frac{c}{G}\,\frac{S}{M^2} \qquad \text{and} \qquad q = \frac{c^4}{G^2}\,\frac{Q}{M^3} \tag{10}$$

of the BH can be determined, where S is the angular momentum and Q the quadrupole moment. These measured properties of a BH can be confronted with predictions of GR.

In GR, the curvature of space-time diverges at the centre of a BH, producing a singularity, which physical behaviour is unknown. The Cosmic Censorship Conjecture was invoked by Penrose in 1969 (see e.g. [30]) to resolve the fundamental concern that if singularities could be seen from the rest of space-time, the resulting physics may be unpredictable. The Cosmic Censorship Conjecture proposes that singularities are always hidden within the event

horizons of BHs, so that they cannot be seen by a distant observer. A singularity that is found not to be hidden but "naked" would contradict this Cosmic Censorship. In other words, the complete gravitational collapse of a body always results in a BH rather than a naked singularity (e.g. [31]). We can test this conjecture by measuring the spin of a rotating BH: In GR we expect $\chi \leq 1$. If, however, SKA observations uncover a massive, compact object with $\chi > 1$, two important conclusions may be drawn. Either we finally probe a region where GR is wrong, or we have discovered a collapsed object where the event horizon has vanished and where the singularity is exposed to the outside world.

One may expect a complicated relationship between the spin of the BH, χ, and its quadrupole moment, q. However, for a rotating Kerr BH in GR, both properties share a simple, fundamental relationship [32], i.e. $q = -\chi^2$. This equation reflects the "No-hair" theorem which implies that the external gravitational field of an astrophysical (uncharged) BH is fully determined by its mass and spin. Therefore, by determining q and χ from timing measurements with the SKA, we can confront this fundamental prediction of GR for the very first time.

The best timing precision would be provided by a PSR-BH system with a MSP companion. Such systems do not evolve in the standard scenarios described earlier, but they can be created in regions of high stellar density due to exchange interactions. Prime survey targets would therefore be the innermost regions of our Galaxy and Globular Clusters. Finding pulsars in orbits around massive or super-massive BHs would allow us to apply the same techniques for determining their properties as for the stellar counterpart [28]. Since the spin and quadrupole moment of a BH scale with its mass squared and mass cubed, respectively, relativistic effects would be measured much easier.

The described tests have been identified as one of the key-science projects for the SKA. More details can be found the SKA science case discussing this and the other key science projects extensively [33–35].

9. Conclusions

The double pulsar system is the most magnificent laboratory to study GR and alternative theories of gravity to date. It goes well beyond – in precision and types of tests – what has been possible in the past. Amazing results are already available and the double pulsar's potential has not been even fully explored. It is a beautiful example how pulsars provide some of the most stringent and in many cases the only constraints for theories of relativistic gravity in the strong-field regime. Being precise clocks, moving in deep gravitational potentials, they are a physicist's dream-come-true. The SKA will provide yet another leap in our understanding of relativistic gravity and hence in the quest for quantum gravity.

Acknowledgments

The author wants to thank the organiser for an inspiring summer school and their support.

References

[1] M. Burgay, N. D'Amico, A. Possenti, R. N. Manchester, A. G. Lyne, B. C. Joshi, M. McLaughlin, M. Kramer, J. M. Sarkissian, F. Camilo, V. Kalogera, C. Kim, D. R. Lorimer, *Nature* **426** 531–533 (2003).
[2] A. G. Lyne, M. Burgay, M. Kramer, A. Possenti, R. N. Manchester, F. Camilo, M. McLaughlin, D. R. Lorimer, B. C. Joshi, J. E. Reynolds, P. C. C. Freire, *Science* **303** 1153–1157 (2004).
[3] S. E. Thorsett, D. Chakrabarty, *ApJ* **512** 288–299 (1999).
[4] J. R. Oppenheimer, G. Volkoff, *Phys. Rev.* **55** 374–381 (1939).
[5] V. E. Zavlin, G. G. Pavlov, *A&A* **329** 583 (1998).
[6] G. F. Bignami, P. A. Caraveo, A. de Luca, S. Mereghetti, *Nature* **423** 725 (2003).
[7] T. H. Hankins, J. S. Kern, J. C. Weatherall, J. A. Eilek, *Nature* **422** 141–143 (2003).

[8] A. G. Lyne, R. S. Pritchard, F. G. Smith, *MNRAS* **265** 1003–1012 (1993).
[9] M. Kramer, A. G. Lyne, G. Hobbs, O. Lohmer, P. Carr, C. Jordan, A. Wolszczan, *ApJ* **593** 31 (2003).
[10] M. D. Young, R. N. Manchester, S. Johnston, *Nature* **400** 848–849 (1999).
[11] M. A. Alpar, A. F. Cheng, M. A. Ruderman, J. Shaham, *Nature* **300** 728–730 (1982).
[12] C. Will, *Living Reviews in Relativity* **4** 4 (2001).
[13] T. Damour, J. H. Taylor, *Phys. Rev. D* **45** 1840–1868 (1992).
[14] R. N. Manchester, A. G. Lyne, F. Camilo, J. F. Bell, V. M. Kaspi, N. D'Amico, N. P. F. McKay, F. Crawford, I. H. Stairs, A. Possenti, D. J. Morris, D. C. Sheppard, *MNRAS* **328** 17–35 (2001).
[15] V. Kalogera, C. Kim, D. R. Lorimer, M. Burgay, N. D'Amico, A. Possenti, R. N. Manchester, A. G. Lyne, B. C. Joshi, M. A. McLaughlin, M. Kramer, J. M. Sarkissian, F. Camilo, *ApJ* **601** L179–L182 (2004).
[16] J. M. Weisberg, J. H. Taylor, The Relativistic Binary Pulsar B1913+16, in: M. Bailes, D. J. Nice, S. Thorsett (Eds.), Radio Pulsars, Astronomical Society of the Pacific, San Francisco, 2003, pp. 93–98.
[17] I. H. Stairs, S. E. Thorsett, J. H. Taylor, A. Wolszczan, *ApJ* **581** 501–508 (2002).
[18] M. Kramer, K. M. Xilouris, A. Jessner, D. R. Lorimer, R. Wielebinski, A. G. Lyne, *A&A* **322** 846–856 (1997).
[19] M. A. McLaughlin, A. G. Lyne, D. R. Lorimer, A. Possenti, R. N. Manchester, F. Camilo, I. H. Stairs, M. Kramer, M. Burgay, N. D'Amico, P. C. C. Freire, B. C. Joshi, N. D. R. Bhat, *ApJ* **616** in press (astro-ph/0408297) (2004a).
[20] M. A. McLaughlin, M. Kramer, A. G. Lyne, D. R. Lorimer, I. H. Stairs, A. Possenti, R. N. Manchester, P. C. C. Freire, B. C. Joshi, M. Burgay, F. Camilo, N. D'Amico, *ApJ* **613** L57 (2004b).
[21] T. Damour, R. Ruffini, *Academie des Sciences Paris Comptes Rendus Ser. Scie. Math.* **279** 971–973 (1974).
[22] B. M. Barker, R. F. Oconnell, *ApJ* **199** L25–L26 (1975).
[23] M. Kramer, *ApJ* **509** 856–860 (1998).
[24] J. M. Weisberg, J. H. Taylor, *ApJ* **576** 942–949 (2002).
[25] N. Wex, *Class. Quantum Grav.* **12** 983 (1995).
[26] T. Damour, G. Schäfer, *Nuovo Cim.* **101** 127 (1988).
[27] T. Damour, G. Esposito-Farèse, *Phys. Rev. D* **58 (042001)** 1–12 (1998).
[28] N. Wex, S. Kopeikin, *ApJ* **513** 388–401 (1999).
[29] N. Wex, *MNRAS* **298** 997–1004 (1998).
[30] S. W. Hawking, R. Penrose, *Royal Society of London Proceedings Series A* **314** 529–548 (1970).
[31] R. M. Wald, General relativity, Chicago: University of Chicago Press, 1984.
[32] K. S. Thorne, R. H. Price, D. A. Macdonald, Black Holes: The Membrane Paradigm, New Haven: Yale Univ. Press, 1986.
[33] M. Kramer, D. C. Backer, J. M. Cordes, T. J. W. Lazio, B. W. Stappers, S. Johnston, Strong-field gravity tests using pulsars and black holes, in: C. Carilli, S. Rawlings (Eds.), Science with the Square-Kilometer-Array (SKA), Elsevier Science Publishers, 2004.
[34] J. M. Cordes M. Kramer, T. J. W. Lazio, B. W. Stappers, Pulsars as Tools for Fundamental Physics & Astrophysics, in: C. Carilli, S. Rawlings (Eds.), Science with the Square-Kilometer-Array (SKA), Elsevier Science Publishers, 2004.
[35] C. Carilli, S. Rawlings, Science with the Square-Kilometer-Array (SKA), Elsevier Science Publishers, 2004.